



Monitoring MCM-41 synthesis by X-ray mesostructure analysis



Sergei D. Kirik^{a,b,*}, Vladimir A. Parfenov^b, Sergei M. Zharkov^{a,c}

^aSiberian Federal University, Krasnoyarsk 660041, Russian Federation

^bInstitute of Chemistry and Chemical Technology SB RAS, Krasnoyarsk 660036, Russian Federation

^cKirensky Institute of Physics SB RAS, Krasnoyarsk 660036, Russian Federation

ARTICLE INFO

Article history:

Received 8 February 2014

Received in revised form 24 March 2014

Accepted 6 April 2014

Available online 16 April 2014

Keywords:

Mesostructure

Hydrothermal stability

MCM-41

X-ray diffraction

TEM

ABSTRACT

The electron density maps calculated from X-ray diffraction patterns of the mesoporous silica material MCM-41 present averaged mesostructure images which in contrast to transmission electron microscopy (TEM) images are exceptionally repeating and represent the whole sample. It was shown that the averaged mesostructure parameters such as a unit cell parameter, a pore diameter, a wall width, a pore shape estimated from the X-ray powder diffraction data in combination with the continuous electron density function approach allow monitoring continuous set of the silica framework states at different stages of the material synthesis.

The mentioned technique supplemented by N₂-adsorption measurements and transmission electron microscopy was applied for consideration of the MCM-41 hydrothermal stability. Attention has been given to the variations of the synthesis conditions affecting the hydrothermal stability, in particular the maintaining the basicity of the synthesis solution as well the substitution of the synthesis solution with water or a salt solution at hydrothermal treatment. The averaged pore shape was observed to be changed from cylindrical to hexagonal-prismatic form. The observed wall thickness was in the range from 0.75 to 1.25 nm. The competition of silica polycondensation and surface hydrolysis was shown to be responsible for the variety of framework geometry and hydrothermal stability. It has been established that the pore diameter increases generally due to the osmotic pressure of water. If the pores acquire the average prismatic hexagonal shape, the sample has low hydrothermal stability. Under the conditions favorable for the polycondensation the pores have averaged cylindrical shape and material demonstrates higher hydrothermal stability. Cooperative mechanism of mesostructure destruction under hydrothermal conditions was observed using TEM data and was discussed in connection with irregular polycondensation.

© 2014 Elsevier Inc. All rights reserved.

1. Introduction

The development of template synthesis methods used in obtaining zeolites and aluminophosphate having a framework structure [1–2] has provided the discovery of mesostructured mesoporous silicates known also as ordered mesoporous silica (OMS) [3–4]. Crystallographically ordered empty space in OMS is organized in uniform shaped and sized pores. The possible range of the pore diameter is within 2–15 nm. The specific surface of the silicate materials reaches up to 1200 m²/g. These characteristics determine the perspective of applying OMS in industry and new branches of technology [5–9]. The detailed description of OMS can be found in a number of comprehensive reviews [10–14].

The low OMS hydrothermal stability (HS) hinders material applications. It was intensively discussed in literature [15–26].

The detailed analysis of the differences between zeolites and OMS including HS can be found e.g. in [14]. However the modern understanding of the OMS nature does not enable one to answer the question how to obtain OMS with the zeolite stability [15]. The efforts made to increase HS followed two directions. The first direction deals with the methods without changing the chemical composition of the final material. They include pH control during the synthesis and hydrothermal treatment procedure [16–21], the control of the ionic strength of the synthesis solution [18,20,22,23], varying the time and changing the temperature of the hydrothermal treatment [20,24–26], changing the conditions and techniques for removing the template [27], the application of more thermo-resistant fluorinated templates and creation of more severe conditions of the hydrothermal treatment [28]. The second direction is connected with doping silica by different chemical elements [13–14,16,17,20,29–31]. Numerous literature data indicate that the synthesis conditions can significantly change the properties of the materials.

* Corresponding author at: Siberian Federal University, Krasnoyarsk 660041, Russian Federation. Tel.: +7 39124954663.

E-mail address: kiriksd@yandex.ru (S.D. Kirik).

The substance structure in the final as well as intermediate points of the synthesis can give substantial basis for understanding the material properties. Modern research methods: nuclear magnetic resonance, transmission electron microscopy (TEM), X-ray diffraction, N₂-adsorption allow in some extent to control the OMS structure on molecular and mesoscale level. The most flexible method to investigate the transformation route seems to be X-ray diffraction. There are a number of papers studying mesophase transformation “in situ” [32–40]. The hexagonal mesophase was shown to form within the first three minutes of the reaction [39]. The time-resolved X-ray diffraction was applied to follow phase transitions in silica/surfactant composites under hydrothermal conditions [37]. The energy-dispersive X-ray diffraction was used to investigate “in situ” formation of the mesoporous silica FSM-16 and MCM-41 in [40]. There are also some details concerning SBA-15 mesophase formation [33,36,41].

However experimental X-ray diffraction data without processing provide only evidences regarding a substance transformation. The question is to transform these data to the information suitable for discussion of chemical processes. The solution is in application of X-ray structure analysis or more specifically X-ray mesostructure analysis. Four approaches were reported in literature for the quantitative description of X-ray diffraction from mesostructure [3,42,43–49]. Beck et al. in their pioneer work [3] simulated the X-ray pattern of MCM-41 in two ways. In the first approach the model structure was built from the atoms similar to the zeolite framework. The simulated X-ray pattern was rather similar to the experimental one. The atom position refinement was not provided due to the inconsistency of the numbers of structural parameters and reflections. In fact, this approach implements the trials and errors method. The second approach is based on the honeycomb structure resulting from the close packing of hollow cylindrical micelles. Each cylinder was considered to be a scattering unit according to the equation obtained earlier by Oster and Riley [42]. Later, this approach was developed in a number of papers [43–47] with the pore structure described by a set of coaxial cylinders with varying radius and wall density. The method of molecular dynamics applied to amorphous silica packed as hexagonal pores in a two-dimensional lattice was demonstrated in [48]. This approach was not developed further, likely due to the increased requirements for calculation resources.

A more flexible approach to refine the averaged parameters of the mesostructure is based on the application of the continuous electron density approach [49]. The parameters of the electron density function are refined in the least square minimizing procedure. The approach was successfully applied in studying zeolites and OMS with the disordered particles in pore space [49–58].

In this paper the X-ray mesostructure analysis was applied for monitoring MCM-41 synthesis. Hydrothermal stability of the MCM-41 material is essentially discussed in the relation with the averaged mesostructure alteration along the synthesis “pathways”. The considered reaction pathways apparently do not cover the whole possible multidimensional space of the states. The choice has been made to touch upon the most intensively discussed in literature variants of the chemical modification of the synthesis solution aimed at increasing the hydrothermal stability. The paper considers the consequences of the mother liquid substitution under hydrothermal treatment. Ammonia and sodium hydroxide as the basicity agents have been compared. The results on the additional silicate deposition on the inner surface of the material in order to increase its stability are reported. The alterations of the mesostructure at certain synthesis stages were followed by the X-ray diffraction data and TEM images. The final materials at each pathway were tested for the hydrothermal stability. The

N₂-adsorption measurements of the texture characteristics have been made, if appropriate, in addition to the X-ray analysis.

2. Experimental

2.1. Chemical reagents and synthesis

The following chemicals were used for synthesis without additional purification: cetyltrimethylammonium bromide C₁₆H₃₃(CH₃)₃NBr (CTABr) – Aldrich (Cat.:85.582-0); tetraethoxysilane Si(C₂H₅O)₄ (TEOS) – analytically pure, technical standards 6-09-3687-74; sodium silicate Na₂SiO₃·9H₂O – REAHIM 130159 All-Union Standard 4239_77; ammonium NH₃ – solution 13.4 M, $\rho = 0.905 \text{ g/cm}^3$, ethanol C₂H₅OH (EtOH) – 96 wt.%, sulphuric acid H₂SO₄ – (98%), potassium chloride KCl – 1 M solution.

All the synthetic experiments were divided into series, with each including several stages namely: precipitation – «aging» (stage 1); hydrothermal treatment in the autoclave (HTT1) (stage 2); removing the template by calcination (stage 3); testing the hydrothermal stability by autoclave exposition of the material in water at 110 °C (HTT2) (stage 4). All obtained samples denoted as: *N/K*, where *N* – the series number and *K* – the stage number, were taken for the X-ray diffraction analysis. In series 1–5 the first stage was carried out in alcohol-ammonia solution with the molar ratio of the components being 1TEOS:0.2CTABr:21NH₃:50C₂H₅OH:475H₂O in accordance with [59]. When preparing the synthesis mixture the weighed quantity CTABr was dissolved in aqueous-alcohol solution with the addition of ammonia up to pH 12.5. After the homogenization TEOS was added into CTABr solution. The precipitation and primary condensation of the product were performed at intensive stirring for 2 h at *t* = 22 °C (stage 1/1). Further stages in series 1–5 had some differences. In series 1 the precipitated product with the mother liquid was placed into an Teflon fettle autoclave to carry out the hydrothermal treatment (HTT1) at *t* = 120 °C for 2 h. After HTT1 the precipitate was filtered, dried at ambient conditions (stage 1/2). The calcination in order to remove the template was made in air at 550 °C for 6 h (stage 1/3). After calcination the substances in all series were tested for the hydrothermal stability (HTT2) by static autoclave exposition at 110 °C for 2 h with the ratio $V_{\text{liquid}}(\text{H}_2\text{O})/m_{\text{solid}}(\text{SiO}_2) = 5 \text{ ml}/50 \text{ mg}$ (stage 1/4). The stage HTT2 was used as a “quality” test to show if a mesostructure was stable or not, however it could be also applied for quantitative characteristic of stability.

In series 2 at stage 2/2 when carrying out HTT1 the mother liquid was substituted with water. In series 3, 1 M solution of KCl was used for this purpose. The HTT1 and HTT2 conditions, such as duration, temperature, stirring, degree of the autoclave filling, were similar in all the cases.

In series 4 and 5 the substance obtained according to stages 1/1–1/3, was additionally treated by silicate reagents in order to coat the surface with an additional silica layer. In series 4 at stage 4/4 the substance was soaked in tetraethoxysilane, followed by its hydrolysis by water in accordance with [60]. Then, the sample was calcinated at 550 °C (stage 4/5) and the hydrothermal stability tested in HTT2 (stage 4/6). In series 5 the material was put into the aqueous solution of sodium silicate with pH 12.5 and subjected to autoclaving for 2 h at 110 °C (stage 5/4). At stage 5/5 the substance was calcinated and HTT2 was carried out (stage 5/6).

Since the silica source influences significantly the product properties [19,20,61], the mesophase precipitation using sodium silicate was investigated in 6 and 7 series. The pH of sodium silicate solution was adjusted by concentrated sulfuric acid at pH 12.5. Stages 6/2, 6/3 and 6/4 regime (in particular temperature and duration) was the same as in series 1. At stage 7/2 (HTT1 stage)

the water-alkaline synthesis solution was substituted with alcohol-ammonia solution identical to stage 1/2.

2.2. X-ray diffraction studies

The X-ray patterns were taken using the diffractometer X'Pert Pro (PANalytical) with the $\text{CuK}\alpha_{1,2}$ radiation and detector PIXcel with a graphite monochromator. Scanning was performed in the angle range of $1\text{--}10^\circ 2\theta$, with the step being 0.026° and counting time – 150–200 s/step. The primary beam overflow was controlled using the divergence slit of $1/16^\circ$ size. The samples for scanning were prepared by dusting fine powder on the nonreflecting silicon plate. The comparison of the X-ray patterns obtained using laboratory diffractometer and synchrotron source presented in [53]. It has shown the peak intensities and positions obtained applying the laboratory diffractometer in the region higher 1° were not distorted, however peak widths were in 2–2.5 times broader.

The X-ray patterns were treated using the full profile technique. The diffraction lines were simulated using the pseudo-Voigt function. The pore shape was simulated by the continuous function of the electron density constructed from a set of concentric circular areas with varying radius, density and shape from a cylinder to a hexagonal prism. The model used permitted up to three areas. The electron density $\rho(x,y)$ was performed as a function:

$$\rho(x,y) = \sum_{m=1}^3 \rho_m [1 + th((R(x,y) - r_m - h_m \delta(x,y)))]$$

where $R(x,y)$ was the distance of the (x,y) point from the center of pore; r was the refining radius of the cylinder with regulated density ρ_m . Each area could continuously transform from the circular into hexagonal shape by means of the refinable parameter of

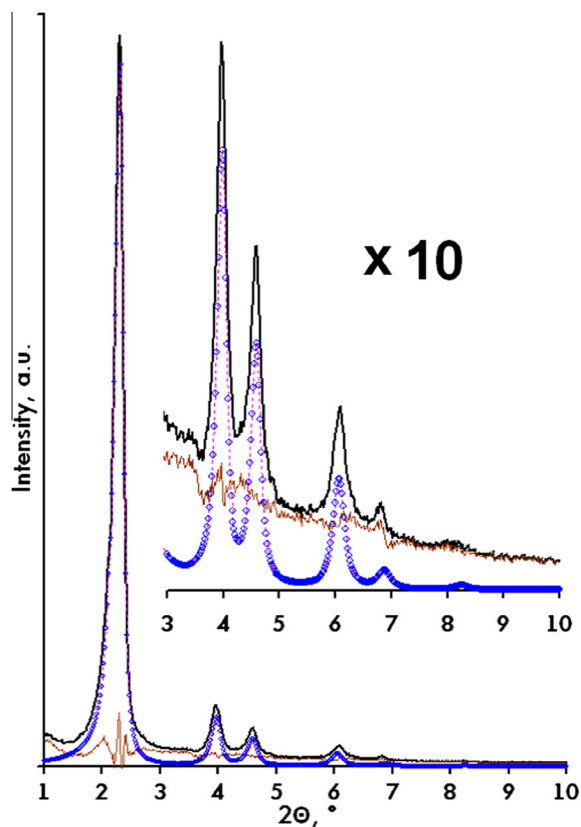


Fig. 1. Simulated (dots) and experimental (thick line) X-ray diffraction patterns of MCM-41 at the first stage of all series. Thin line is the difference between the experimental and simulated X-ray patterns.

«hexagonality» h being varied from 0 to 1 in combination with $\delta(x,y)$. The refinable thermal Debye–Waller parameter took into consideration the sharp decrease of the reflection intensity caused by the average pore deformation. The detailed description of the model is presented in [49]. The structural factors for the reflections in the scanning area were calculated by numerical integrating over the independent area of the two-dimensional cell according to:

$$F(hk) = \frac{1}{S_0} \int_{S_0} \rho(x,y) \exp(2\pi i(hx + ky)) dx dy$$

The number of the structural amplitudes, involved in calculation, varied from sample to sample from 5 to 8. The model parameters were refined using the full profile of the X-ray pattern by the method of differential difference minimization [62]. Fig. 1 presents the correspondence of the simulated and experimental X-ray diffraction patterns for the sample (1/1) as an example. The electron density maps (Fig. 2) were calculated from the structural amplitudes estimated from the X-ray patterns. The signs of the structural amplitudes were obtained at the stage of modeling and refinement. The wall thickness was defined as the difference between the cell parameter and diameter of the silica ring (Table 1). The accuracy

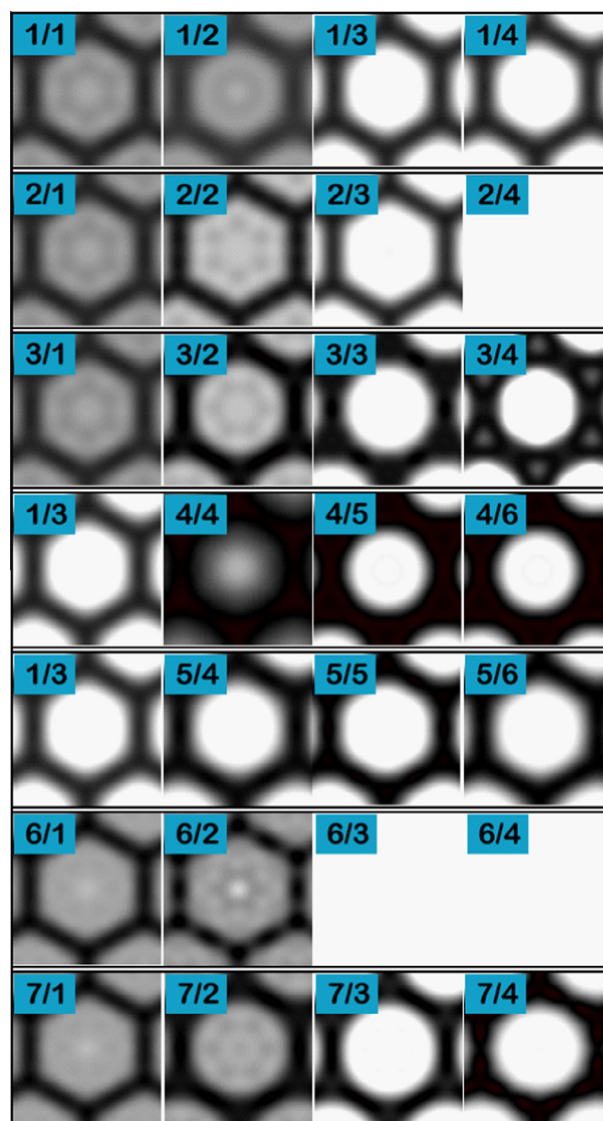


Fig. 2. Electron density maps for the samples of series 1–7.

Table 1
Structural and texture parameters of the samples of series 1–7.

Series/stage	a_0 (nm)	r_1/r_2 (nm)	d (nm)	h_1/h_2 (%)	ρ_1/ρ_2	B_1/B_2 (nm ²)	R_{wp} (%)	S (m ² /g)
1/1	4.478	1.79/0.33	0.89	59/0	20/7.4	0.24/3.16	8	
1/2	4.473	1.72/0.27	1.04	60/0	20/6.1	2.15/0.43	7.7	
1/3	4.369	1.71/-	0.95	46	20/-	1.23/-	8.3	1143
1/4	4.353	1.71/-	0.94	46	20/-	1.00/-	11.5	978
2/1	4.478	1.79/0.33	0.89	59/0	20/7.4	0.24/3.16	8	
2/2	4.742	1.97/0.28	0.81	100/0	20/2.3	3.16/0.31	9.7	
2/3	4.423	1.79/-	0.84	52/-	20/-	0.59/-	9.5	1204
2/4	Disordered material							
3/1	4.478	1.79/0.33	0.89	59/0	20/7.4	0.24/3.16	8	
3/2	4.602	1.82/0.28	0.96	57/0	20/3.4	3.14/2.71	10.5	
3/3	4.130	1.57/-	0.98	23/-	20/-	1.99/-	8.8	1062
3/4	4.076	1.42/-	1.23	33/-	20/-	0.61/-	15.6	594
4/1	4.478	1.79/0.33	0.89	59/0	20/7.4	0.24/3.16	8	
4/2	4.473	1.72/0.27	1.04	60/0	20/6.1	2.15/0.43	7.7	
4/3	4.369	1.71/-	0.95	46/-	20/-	1.23/-	8.3	1143
4/4	4.263	Not calculated						22
4/5	4.264	1.51/-	1.25	0/-	20/-	3.00/-	7.7	449
4/6	4.259	1.51/-	1.25	0/-	20/-	3.00/-	12.8	218
5/1	4.478	1.79/0.33	0.89	59/0	20/7.4	0.24/3.16	8	
5/2	4.473	1.72/0.27	1.04	60/0	20/6.1	2.15/0.43	7.7	
5/3	4.369	1.71/-	0.95	46/-	20/-	1.23/-	8.3	1143
5/4	4.367	1.64/-	1.09	62/-	20/-	2.32/-	8.1	-
5/5	4.322	1.69/-	0.95	57/-	20/-	1.25/-	10.4	840
5/6	4.307	1.64/-	1.02	50/-	20/-	2.72/-	8.4	857
6/1	4.601	1.89/0.33	0.82	90/0	20/7.2	2.08/3.24	5.9	
6/2	4.703	1.98/0.32	0.75	91/0	20/5.9	1.94/2.94	6.6	
6/3	Disordered material							
6/4								
7/1	4.601	1.89/0.33	0.82	70/0	20/7.2	2.08/3.24	5.9	410
7/2	4.507	1.76/0.26	0.99	48/0	20/2.1	2.59/2.43	6.8	269
7/3	4.311	1.70/-	0.90	40	20	0.20	6.8	682
7/4	4.258	1.67/-	0.91	18	20	3.24	21.8	550

Stages: 1 – precipitation and primary condensation; 2 – HTT1; 3 – calcination; 4 – HTT2 (hydrothermal testing). For series 4 and 5: 4/4 – layer deposition; 4/5 – second calcination; 4/6 – HTT2. a – lattice parameter; r_1, r_2 – radii of the circular areas of the electron density; d – pore wall thickness; h_1, h_2 – degree of the pore hexagonality of the circular areas; ρ_1/ρ_2 – relative densities of the circular areas; B_1/B_2 – thermal parameters; R_{wp} – fitting reliability factor. S – specific surface (BET).

of the estimation of the lattice parameter was 0.005 nm and the estimation of the pore wall thickness varied within 0.04 nm. The hexagonality degree was determined with the deviation of 15%.

2.3. Sorption measurements of the surface

The specific surface was measured at stages 3 and 4 for 1–3, 6, 7 series and at stages 5 and 6 for 4 and 5 series by the nitrogen adsorption using Micromeritics ASAP 2420. The preliminary sample degassing was made at 300 °C for 8 h in deep vacuum ($P \sim 10^{-6}$ pa). The nitrogen sorption–desorption isotherms were registered at 77 K in the range of p/p_0 (0.01–0.99). The specific surface was calculated using the model BET [63].

2.4. TEM measurements

Transmission electron microscopy images were obtained using JEOL JEM-2100 at accelerating voltage of 200 kV. Studied powder sample of MCM-41 was dispersed in isopropyl alcohol, using an ultrasonic bath. Then, a drop with suspended particles was deposited on a thin carbon film supported by TEM grid.

3. Results and discussion

There are a lot of TEM images published in the literature convincing in the regularity of OMS structure. In the case of MSM-41 two-dimensional periodicity of the material allows one to see the spatial location of main construction elements and generally interpret the structure. A detailed examination of TEM images detects individuality of almost every pore. It, however, does not destroy

the concept of substance structure. Presented in Fig. 3(a–c) TEM images of the sample (3/4) obtained from different particles of the material evidence about both the similarities and differences in the local structure. The X-ray powder diffraction pattern of the substance (e.g. Fig. 1) in contrast to TEM images is exceptionally repeating, and represents the averaging structure for the whole sample. It should be noted that the limited number of reflections on the X-ray pattern is the consequence of the local individuality in structure too. The electron density maps (E-map) applied in the present paper is a product of calculation, made from X-ray diffraction data. It intends to give a scheme of the geometrical structure of the matter. The resulting picture is an averaged structure which is different from every specific pore. However, the E-map is able to respond to fine quantitative changes on the X-ray powder diffraction pattern, converting them into information suitable for considering the consequence of synthesis conditions on the substance properties. One should be aware that the averaging distorted sections of the structure may create artifacts. Especially it is expectable for the situation where three dimensional objects are described with two dimensional models. For this reason, the interpretation of electron density maps should, if possible, be considered with other data. In this study E-maps were applied to interpret the changes in hydrothermal properties of MCM-41 caused by synthesis conditions. With this purpose the alterations of some averaged structure parameters derived from E-maps were investigated in seven multistage experiments of MCM-41 synthesis.

The obtained results show that there are a continuous set of silica framework states at different stages of the material synthesis. The framework evolution can be considered taking into account the lattice parameter value, wall thickness, pore shape which is

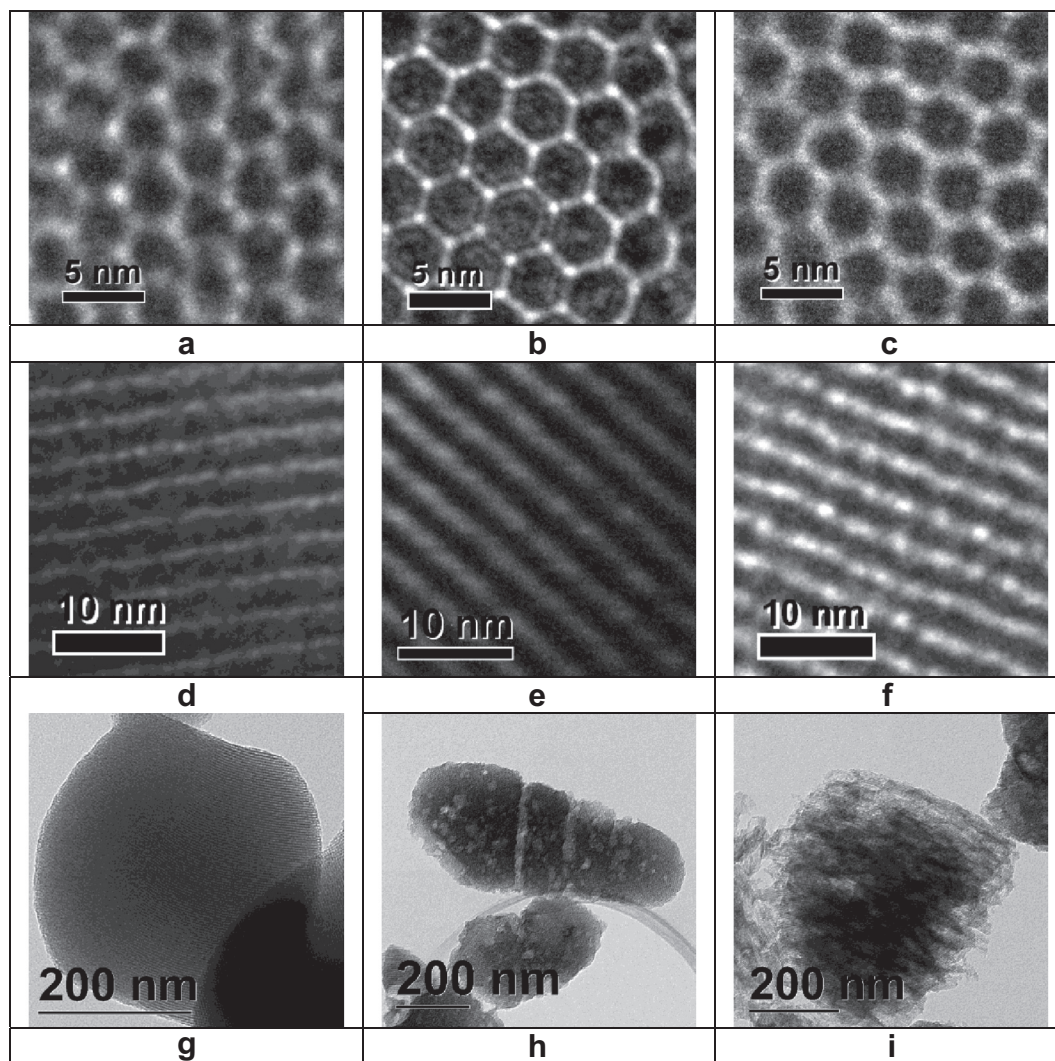


Fig. 3. a,b,c – TEM images of the sample (3/4) obtained from different particles viewed perpendicular to the hexagonal pore arrangement; d,e,f – TEM images of different samples: d – sample (1/2), e – sample (2/2), f – sample (3/4) viewed along the direction of the hexagonal pore arrangement; g,h,i – stages of particles degradation under hydrothermal treatment; g – initial particles, h – particle with spots of local degradation, i – particle before destruction.

capable to change from the regular hexagonal prism to cylinder, the size of the cylindrical area occupied by the organic template. Table 1 presents the numerical structural characteristics and Fig. 2 additionally shows the electron density maps for the cases where the map calculation was possible.

3.1. Series 1: regular synthesis in alcohol-ammonia solution

Series 1 presents an optimized variant of the MCM-41 synthesis in the alcohol-ammonia solution [65,66]. The synthesis requires the minimal time about 3–4 h. The product demonstrates good hydrothermal stability [59]. The monotonic decrease of the lattice parameter and pore radius at all observation points indicates the fact that at each stage the silicate polyanions are converging, likely, due to the polycondensation. The wall thickness changes non-monotonically. At stage HTT1 (1/2) wall thickness increases on 0.15 nm as opposed to stage (1/1). Observation made hardly demonstrates real wall broadening. The important arguments are that there are no silicate particles in the synthesis solution which are able to increase the wall size on 0.15 nm. Seemingly, the contribution to the wall thickness change makes a ripple effect or unevenness along the pore axis decreasing pore diameter, which was observed by the TEM-tomography for SBA-15 [67]. Irregular pulsation of the pore diameter can also be observed for MCM-41 using

TEM images with the pore orientation in the picture plane (Fig. 3(d–f)). The phenomenon of the apparent wall broadening at the HTT1 stage was also revealed in series 3 and 7 (stages 1/2, 3/2, 7/2, (Table 1)). It correlates with the hydrothermal stability increasing. The observed wall roughness can be interpreted as partial and local polycondensation processes along wall surface. This irregularity leads to decreasing the local pore radius and hexagonality, increasing the apparent wall thickness. Discussing polycondensation it is also reasonable to distinguish two main orientations of (Si–O–Si) bonds in the wall body: along wall surface and perpendicular to wall surface i.e. along the pore radius. The silica polycondensation inside the pore wall volume proceeds intensively at calcination, resulting in the decrease of the wall thickness (stages 1/3 and 7/3) and the cell parameter too.

The template can be seen in the inner area of the electron density map. It occupies almost the whole pore space (>95%). The central small cylindrical area with the diameter of about 0.3 nm is not occupied. The X-ray diffraction revealed that the template was only slightly washed out from the pores during 2 h of HTT1. The diminishing weight lost at calcination in the range 2–3% pointed out the template leaching at HTT1 too. The pore hexagonality at stages 1/1 and 1/2 was the same, allowing conclude that the template did not induce any considerable pressure on the pore wall at HTT1 in the mother liquid solution. The result of

HTT2 stage (1/4) evidenced that the material obtained was resistant to a hydrothermal impact. The decreasing of the value of specific surface (15%) at HTT2 can approximately be brought into agreement with the portion of the mesophase decay [68].

3.2. Series 2: the synthesis with hydrothermal treatment in water solution

When substituting the alcohol-ammonia synthesis solution (mother liquor) with water at HTT1 stage (2/2) considerable structural changes were observed. The lattice parameter increased by approximately 5%. The pore took the shape of a regular hexagonal prism (Table 1, Fig. 2). The calcination stage (2/3) resulted in strong lattice compression. The considerable changes of the framework signify the low degree of the silica polycondensation. As a result at HTT2 stage (2/4) the mesostructure was entirely destroyed. The hexagonal shape and radius increased after HTT1 (2/2) indicated that the pressure arisen in the pore and was not balanced with “polycondensation” forces. It is notable that in series 1 the pressure in pores did not manifest itself at the HTT1 stage (1/2) at the same medium temperature. The comparison of the conditions for series 1 and 2 makes it possible to claim that the thermal expansion of the template cannot be the cause of the pore expansion. Therefore, there is some evidence of the template did not induce any considerable pressure inside the pore at this synthesis stage. The explanation based on the growth of the osmotic water pressure in the pores seems to be realistic. Actually, the water in pores as a component of the physical–chemical system has smaller chemical potential than the water outside the pores after the substitution of the mother liquid. It induces active diffusion of water molecules into pores and increases osmotic pressure there. The pore expansion causes pore perimeter increasing more than 1 nm. It results in steric hindrance for the complete silica polycondensation, and, consequently, in low hydrothermal stability. The lattice parameter contraction at calcination showed that the pore expansion at HTT1 was not accompanied with the additional silicate polyanion embedding into the pore wall. It is important to note that polycondensation occurring at calcination did not provide the substance stability (stage 2/4).

3.3. Series 3: the synthesis with hydrothermal treatment in KCl solution

In series 3 at HTT1 stage the mother liquor was substituted by 1 M KCl solution. The so-called “salt effect” was repeatedly described in literature [18,21,69] in connection with hydrothermal stability. Although the salt solution inhibits silicate hydrolysis as well as the polycondensation rate, it decreases the osmotic pressure in the pores. Both mentioned factors can change the mesostructure. After HTT1 stage (3/2) the lattice parameter increased approximately two times less than in series 2 (stage 2/2) presumably due to the lower osmotic pressure. The pore hexagonality increased only up to 87%. At calcination stage (3/3) the lattice was greatly compressed (>10%). Approximately only a half of the substance retains mesostructure after HTT2 stage (3/4). The lattice parameter decreasing indicates the polycondensation process. The wall thickness increased up to 0.96 nm at stage 3/2, and, then up to the value 1.23 nm at stage 3/4. The calculated E-map shows cylindrical pore shape at the stage (3/3) (Fig. 2), which became more pronounced after HTT2 stage (3/4). The E-map (3/4) shows additional small empty spaces formed by the contact of three adjacent cylinders (Fig. 2). The appearance of additional pores on the electron density map was a result of distinctive changes in X-ray diffraction pattern. The intensity of the second reflection becomes lower than that of the third one (Fig. 4). The described diffraction effect is rather unusual for MCM-41 but quite typical for SBA-15.

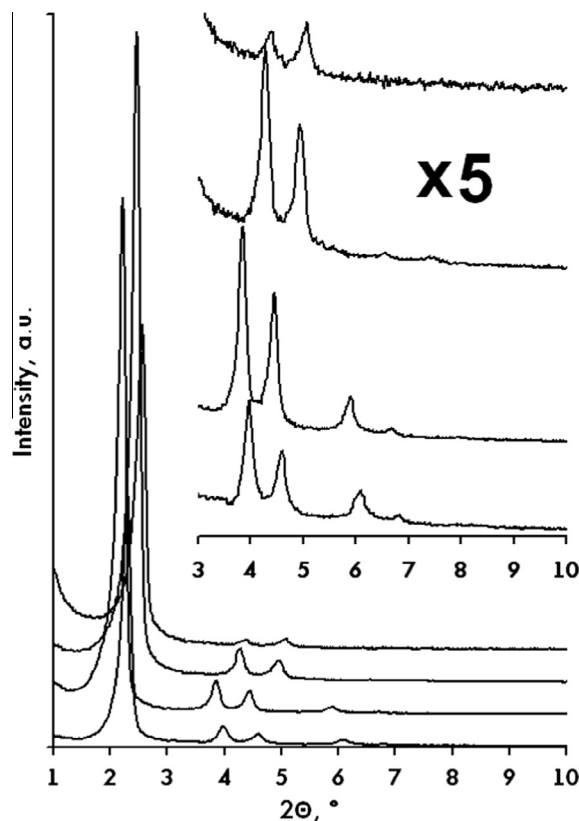


Fig. 4. X-ray diffraction patterns of MCM-41 at the all stages (3/1, 3/2, 3/3, 3/4) of series 3.

The first interpretation of the intensities inversion was given in [70], where SBA-15 structure model with additional circular corona area around the pore was suggested. Later, the electron density simulation for SBA-15 was repeated in [36] and confirmed by TEM data [32,33]. It was shown that the process of SBA-15 formation followed through the stages of separate spherical and then individual cylindrical micelles. In this respect the observation of dense cylinder parking seems to be realistic situation.

Several experiments have been carried out to validate the retained effect of the individual cylinders observed on the E-map for sample (3/4). Low temperature N_2 -adsorption have been applied to detect presumable microporosity in the substance. However the measurement have shown the micropore absence. It can be explained also by closeness of expected pore diameter (about 0.4 nm) to the size of adsorbed N_2 -molecules (about 0.386 nm). It makes microporosity measurement difficult. Two molecular models of MCM-41 with hexagonal and cylindrical pores were prepared and X-ray powder patterns were simulated (Fig. 5). The calculation confirms the intensity flipping effect for of the second and third reflection for the sample (3/4). One of the models which can explain the transformation of hexagonal pores to cylindrical one is presented in Fig. 6. If to spin the top and the bottom of the hexagonal prism in opposite directions the inner space would transform from prism to cylinder.

Some evidences were obtained from TEM data. In Fig. 3(a–c) there are TEM images obtained from various particles of the sample (3/4). Regardless of different perfection of particles it is impossible to see any additional pores in the space of contact of the three nearest cylinders. Pores have hexagonal-prismatic shape. The wall of the pores is hardly to be broadened. Nevertheless, taking into account that the observation presents exclusively particle surface, one cannot make a conclusion about the pore structure at full length of the channel. TEM images for the samples (1/2), (2/2)

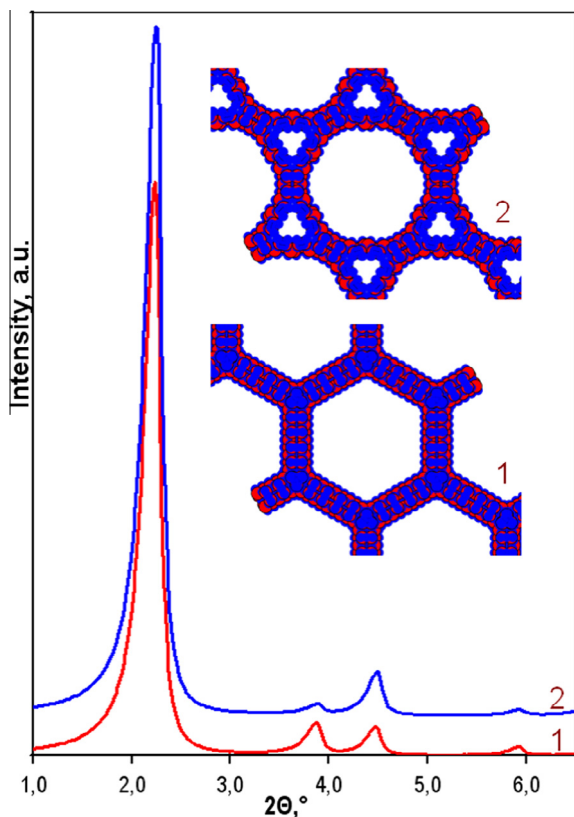


Fig. 5. The molecular models of MCM-41 with hexagonal and cylindrical pores and corresponding simulated X-ray powder patterns.

and (3/4) presented in Fig. 3(d–f) demonstrate various smoothness of mesopore channels. Sample (1/2) corresponds to the standard synthesis condition. In case of (2/2) the most perfect structure was achieved due to the high osmotic pressure. The smoothness of the pores in the sample (3/4) is noticeably inferior to the first and second cases. Local roughness of the walls becomes more noticeable. The deviation from the ideal wall position can be estimated in tens percentage of wall thickness. The above discussed uneven surface polycondensation effects, causing the apparent wall broadening, reaches the maximum value in the case of the sample (3/4). The finite areas with a geometrically regular

fragmentation of the walls can be observed in the Fig. 3f. This phenomenon could be attributed to the electron beam defocusing or other instrument effects. However, some additional facts allow to interpret it also as a stage of the mesostructure destruction. Fig. 3(g–i) show the stages of the particle destruction. “Young” particle (sample 1/3, Fig. 3g) with clear smooth boundaries has a form of hardened drop of condensed matter, where liquid crystal template processes have been over. In sample (3/4), besides many typical particles with unusual defects, located inside the particle body (Fig. 3h). Fig. 3i shows a particle at a stage preceding disintegration. Apparently, the observed channel distortions (Fig. 3f) can be precursors to a local site degradation. The decreasing mesostructure lattice parameter (Table 1) at the stage (3/4) means that polycondensation takes place. Presumably, the active polycondensation in the absence of a template leads to a distortion of the pore walls and local destruction. The pore transformation mechanism presented in Fig. 6 seems to be reasonable because of cooperative feature. When the certain pore is spinning it loses the links with neighboring pores. So, it induces a destruction of a whole region. The TEM image in Fig. 3h demonstrates such local regions of destruction. At the beginning stage the apparent wall broadening accompanied by the effect of the appearance of the additional small pores observed at E-map which can be explained by the effect of averaging distorted channels.

3.4. Series 4: the mesoporous surface treatment with TEOS

In series 4 the material obtained according to the standard scheme (stages 1/1–1/3) was “coated” with additional silica to increase the hydrothermal stability (stage 4/4). It was primarily assumed that TEOS would have relatively uniform distribution over the inside surface of the calcinated mesophase and the silica formed after TEOS hydrolysis would form a monomolecular layer. On the X-ray diffraction pattern of sample (4/4) the second (11) and third (20) peaks lose their intensity considerably as compared to the first one (10). The calculated electron density maps reveal blurred and broadened pore walls (Fig. 2, (4/4)). This is expected result because Fourier series for map calculation consists of only one member. This was the reason why pore parameters were not calculated (Table 1). In course of the TEOS hydrolysis simultaneously with the silica deposition the formation of large particles filling the pores was likely to occur. It was confirmed by the decrease of the specific surface value from 1143 m²/g down to 22 m²/g for sample (4/4). Since the mesostructure remains, such

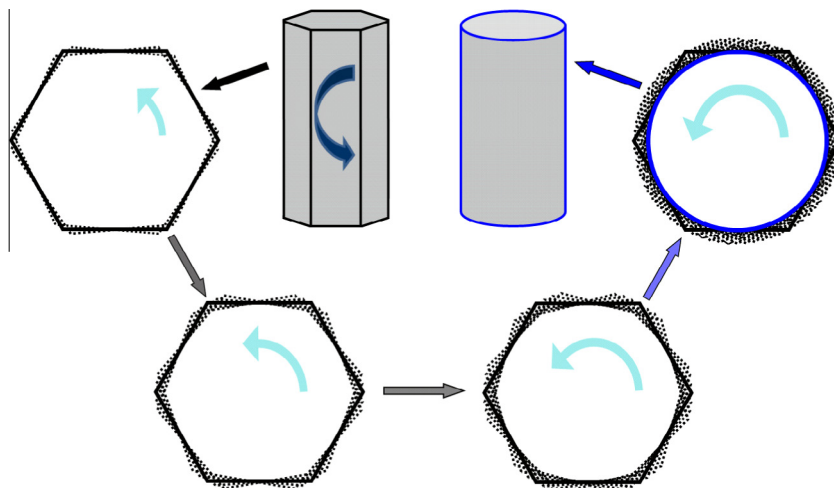


Fig. 6. The transformation of hexagonal pore shape into cylindrical via screw deformation of hexagonal prism. The screw deformation is followed by increasing bonding along surface and bond decaying between adjacent cylinders.

considerable alteration of specific surface value could be explained by the surface being inaccessible for the measurements. Indeed, after calcination (stage 4/5) the specific surface increased up to $449 \text{ m}^2/\text{g}$. The final sample (4/6) has the wall thickness of 1.25 nm which is about 0.4 nm smaller than the expected value for the case of an additional monomolecular silica layer on each side of the wall. Thus, TEOS soaking does not lead to the formation of an additional layer; the silica plugs is located inside the pores preventing the access to the surface.

3.5. Series 5: the mesoporous surface treatment with sodium silicate

A somewhat different situation was observed in series 5, where the treatment was carried out in sodium silicate solution under the conditions of the additional HTT (stage 5/4). The pore wall thickness increased up to 1.09 nm mainly due to the decrease of the pore diameter which might be explained by the deposition of the silicate species on the inside surface. At second calcination (stage 5/5) the wall thickness returned to its initial value (0.95 nm). The specific surface in the course of such procedure of «coating» decreased down to the value of $840 \text{ m}^2/\text{g}$ and after HTT2 (stage 5/6) amounts to $857 \text{ m}^2/\text{g}$. From the point of view of retaining the specific area the sample (5/5) demonstrated the highest stability. It is also possible to note that the degradation rate in (5/5) was lower in comparison with sample (1/3). As a whole, the changes occurring at stage (5/4), can be considered as «healing» (reconstructing) the defective areas of the silica surface.

3.6. Series 6: synthesis in aqueous-alkaline solution

In series 6 and 7 the precipitation of the organosilicate composite (stages 6/1 and 7/1) was carried out in aqueous-alkaline solution. Earlier it was noticed that the aqueous-alkaline synthesis solution led to highly ordered mesostructures [3,60,69], however, their low stability caused doubts in a practical use of MCM-41. Afterward, the synthesis using the alcohol-ammonia solution [64,66,69] rehabilitated expectation from MCM-41. Meanwhile, the reasons of stability improving are not sufficiently explained. The aim of the syntheses in series 6 and 7 was to check the possibility of obtaining a stable product from the aqueous-alkaline solution. Series 6 was similar to series 1, aside from stages (6/1) and (6/2) were carried out in the aqueous-alkaline solution. In series 7 the stage (7/1) was carried out in aqueous-alkaline solution and then at the stage (7/2) the precipitate was placed into alcohol-ammonia solution.

The aqueous-alkaline synthesis solution (stage 6/1) resulted in increasing the lattice parameter as compared to sample (1/1). The framework expansion continued at the stage (6/2). The wall thickness had the smallest value of 0.72 nm and the apparent wall fragmentation was occurred which was likely to indicate the appearance of disruptions in the wall (Fig. 2 (6/2)). The high hexagonality of the pore shape indicated the presence of osmotic phenomena. The reason of the osmosis is believed to be somewhat different. The negative charge of the silicate anions is compensated by the template and, partially, by the sodium cations. After the precipitation there occurs the redistribution of the sodium ions located in the solution and in the pores of composite. Since the inside surface is about 20 times higher than the external one, the localization of the sodium ions (participating in the charge compensation) would be higher inside the pores. Since the pore volume is much smaller than the volume of the synthesis solution the concentration difference of the sodium ions induces the osmotic pressure in the pores. The osmosis contributes to the higher material ordering and, simultaneously, prevents the silica polycondensation due to the steric obstacles for the (Si–O–Si) bond formation. The high ionic strength of the pore solution also inhibits the silicate

hydrolysis and, consequently, the silica polycondensation. Two hour HTT1 (stage 6/2) resulted in the sample decomposing at calcination (stage 6/3). It means that the polycondensation after stages (6/1) and (6/2) was not sufficient for retaining the mesostructure without the organic template and the calcination did not provide the required polycondensation. It is worth to note that the HTT1 stage with duration up to 1–3 days and temperature up to 120–140°C does not increase the hydrothermal stability [66,69].

3.7. Series 7: synthesis in aqueous-alkaline solution with hydrothermal treatment in alcohol-ammonia solution

As to series 7 at HTT1 stage the sample was separated from the mother liquor by filtration and placed into alcohol-ammonia solution (stage 7/2). The lattice parameter after HTT1 decreased more than 0.1 nm. The decreasing continued at the calcination stage (7/3). The wall thickness finally acquired the value of 0.90 nm. Sample 7 retained the mesostructure at HTT2 stage (7/4), however, the specific surface was almost two times smaller. Thus, the aqueous-alkaline medium does not contribute into the silica polycondensation, however its substitution with the alcohol-ammonia or aqueous-ammonia one at the stage of HTT1 allows the synthesis pathway leading to the stable material.

The discussed results convince that the structural data obtained by X-ray powder diffraction correlate with the variations in the chemical synthesis medium and material properties. Despite of a significant individuality of OMS local structure the averaged structure has common features, which alterations could be reasonably interpreted. Hexagonally packed cylindrical pores are the basic element of the structure, which is able to change its settings in limited ranges without the structure destroying. The lattice parameter of 2-dimensional hexagonal unit cell is the most objective structural value with limited extent. Significant variation of the lattice parameter (up to 0.5 nm) at the synthesis stages is an indicator of low hydrothermal stability of the final material. The low silica polycondensation is the obvious reason. Significant growth of the cell parameter is induced by osmotic phenomenon and inhibited polycondensation. Such conditions are realized in aqueous alkaline synthesis solution due to of silica hydrolysis suppressing. Thermal polycondensation that occurs when template is removed by the calcination, does not significantly increase the stability of the material. The width of the pore walls is the next important averaged crystallographic value involved in the consideration. It is derived from the electron density maps calculated from X-ray diffraction data. The width is apparent value sensitive to variations of synthesis conditions. The comparison of E-maps with TEM images implies the cause of its pseudo-reality. Numerous TEM-data obtained on the verge of atomic-molecular discreteness, give a base to assume that the width of the wall is more or less constant. This is in correspondence with the stoichiometry between surfactant and silica at synthesis of OMS. The applying 2-dimensional model to the 3-dimensional object when calculating the E-maps does not take into account changes in the pore diameter or curvature along the channel, which are compensated by the wall thickness and the pore shape. The optimal value of the pore width is in the range 0.8–0.9 nm, which corresponds to the wall built from two layers of $[\text{SiO}_4]$ tetrahedron [66,68]. Cross-section of the two-layer wall is presented in Fig. 7. The lower width than the specified interval is a sign of wall deficiency and the inevitable low hydrothermal stability of the material. Increased wall width is accompanied by the appearance of cylindrical pore shape on E-map that does not fully correspond to TEM images. It can be explained by the increase in surface roughness due to uneven polycondensation. A moderate increase of the apparent width within the interval 1.0–1.1 nm correlates with high hydrothermal stability of the material. The growth of the apparent width, for example, up

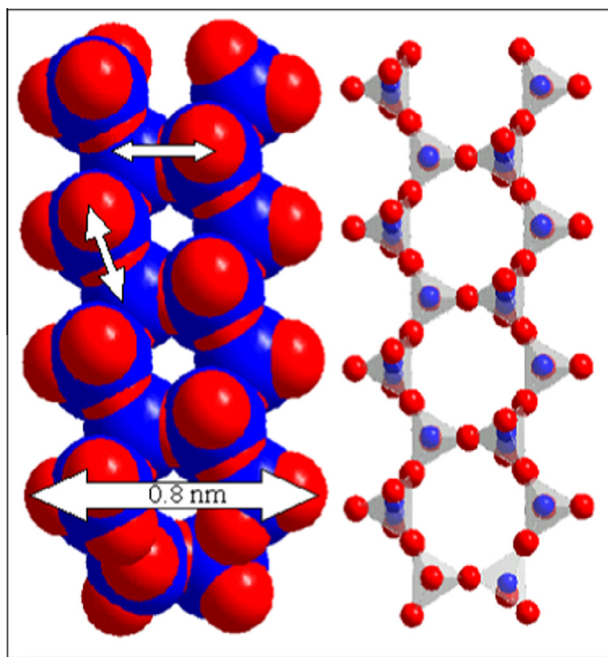


Fig. 7. The pore wall model is presented in two styles. The size of $[\text{SiO}_4]$ tetrahedron, the wall thickness about 0.8 nm, the wall density, the density of silanol groups on the surface are arguments in two layer structure of the wall. The two layer structure suggests two orientations of siloxane bonds $[\text{Si}-\text{O}-\text{Si}]$ along the pore surface and the pore radius shown in the figure. Competition of polycondensation along these directions gives variety of substance states. Detailed model description was presented in [66,68].

to 1.25 nm at hydrothermal treatment with removed template, was the indicator of critical concentration of local defects and roughness of channels. In the limit, the uneven polycondensation causes extensive local defects with the consequent structure collapse (Fig. 3h).

TEM images show that there are a great variety of asymmetrically distorted pores in the substance. The pore shape calculated from X-ray diffraction data presents continuously transitioned figure from the hexagonal-prismatic to the cylindrical form. Mandatory symmetrical and convex form is explained by the applied model. As a perfect hexagonal-prismatic form and all the rest are unrealistic forms. They should be classified as apparent. However, there is a clear correlation between an apparent form and hydrothermal stability. The highly hexagonal form corresponds to the materials obtained in the conditions of high osmotic pressure and therefore they have low hydrothermal stability. The cylindrical shape is a signal of high concentration of local distortions in the pore channels, which is a symptom of the beginning degradation. Hexagonality ranges from 50% to 80% correlates with good hydrothermal stability.

Since a shape of a substance particle is finally supported by chemical bonds it would be relevant to link the apparent structure characteristics obtained from X-ray diffraction data with geometrical orientation of chemical bonds in OMS. Because of the wall thickness is about 0.8–0.9 nm the only two layers of $[\text{SiO}_4]$ -tetrahedrons are allowed to build the wall. This circumstance limits tetrahedron orientation in the layer and allows separating two groups of $(\text{Si}-\text{O}-\text{Si})$ bonds stretched along pore surface and towards pore radius (Fig. 7). The hexagonal-prismatic pore shape is a result of extreme pore expansion at the minimum silica polycondensation along the pore surface. Obviously, the $(\text{Si}-\text{O}-\text{Si})$ bonds along radial direction are not sufficient to provide high material stability. On the contrary the cylindrical shape is characteristic of polycondensation along the surface, where the $(\text{Si}-\text{O}-\text{Si})$ bonds are oriented along pore surface. The cylindrical pore has higher stability.

However, cylindrical shape is the product of averaged local pore roughness. If the roughness exceeds the limit the structure corrosion develops. For these reasons, the cylindrical shape cannot provide maximum stability. So, the material with both orientations of $(\text{Si}-\text{O}-\text{Si})$ bonds otherwise with the intermediate pore shape corresponds to the highest hydrothermal stability. Thus, the synthetic task can be formulated as to suggest synthetic conditions providing comparable rates of polycondensation towards the pore radius and along the surface for reaching the highest density of siloxane bonds.

4. Conclusion

The X-ray diffraction data via apparent structural parameters allow monitoring MCM-41 mesostructure differentiating a great variety of mesophase states in different synthesis pathways. Two chemical reactions silicate hydrolysis and polycondensation occur in the substance after the precipitation and liquid-crystalline templating process. The synthesis conditions influence on the rate of these reactions, induce steric hindrances for polycondensation and result in mesostructure variations. The polycondensation can be accelerated or inhibited in an anisotropic manner. Two directions can be specified along the pore perimeter and along the pore radius. The competition of these two possibilities is responsible for the variety of material properties including hydrothermal stability. When the synthesis is carried out in alcohol-ammonia solution highly ordered material with a high surface area and hydrothermal stability can be obtained. The pores have an averaged intermediate shape between a cylinder and a hexagonal prism. Aqueous and aqueous-alkaline solutions result in highly ordered substances with pores of regular hexagonal shape. However the materials are characterized by the low hydrothermal stability.

In the experiments on the surface coating using TEOS no multiple increase of the wall thickness was observed. The silica species block the pores making them inaccessible. However, if in the solution with a small degree of silica aggregation was applied the effect of the reconstruction of the defective areas of the pore wall was observed resulting in increasing hydrothermal stability. The presented results allow conclude that X-ray mesostructure analysis is effective approach for investigating mesostructured materials.

Acknowledgment

The investigation was made with financial support of the Program of Presidium RAS (Project 24.37), RF State contracts No 02.740.11.0629, RFBR Grants: 11-03-00610a and 11-03-12161-ofi, RSF 14-13-000025.

Appendix A. Supplementary data

Supplementary data associated with this article can be found, in the online version, at <http://dx.doi.org/10.1016/j.micromeso.2014.04.012>.

References

- [1] D.W. Breck, *Zeolite Molecular Sieves, Structure, Chemistry and Use*, John Wiley & Sons, New York, London, Sydney, Toronto, 1974. p. 550.
- [2] M.L. Occelli, H.E. Robson (Eds.), *Synthesis of Microporous Materials: Molecular Sieves*, Van Nostrand Reinhold, 1992. p. 650.
- [3] J.S. Beck, J.C. Vartuli, W.J. Roth, M.E. Leonowicz, C.T. Kresge, K.D. Schmitt, C.T.-W. Chu, D.H. Olson, E.W. Sheppard, S.B. McCullen, J.B. Higgins, J.L. Schlenker, *J. Am. Chem. Soc.* 114 (1992) 10834–10843.
- [4] T. Yanagisawa, T. Shimizu, K. Kuroda, C. Kato, *Bull. Chem. Soc. Jpn.* 63 (1990) 988–992.
- [5] A. Sayari, S. Hamoudi, Y. Yang, *Chem. Mater.* 17 (2005) 212–216.
- [6] P. Kumar, V.V. Gulians, *Micropor. Mesopor. Mater.* 132 (2010) 1–14.
- [7] P.J.E. Harlick, A. Sayari, *Ind. Eng. Chem. Res.* 45 (2006) 3248–3255.

- [8] A. Taguchi, F. Schuth, *Micropor. Mesopor. Mater.* 77 (2005) 1–45.
- [9] A. Walcarius, *Chem. Soc. Rev.* 42 (2013) 4098–4140.
- [10] U. Ciesla, F. Schuth, *Micropor. Mesopor. Mater.* 27 (1999) 131–149.
- [11] R.C. Hayward, P. Alberius-Henning, B.F. Chmelka, G.D. Stucky, *Micropor. Mesopor. Mater.* 44–45 (2001) 619–624.
- [12] A. Walcarius, L. Mercier, *J. Mater. Chem.* 20 (2010) 4478–4511.
- [13] G.J.D. Soler-illia, C. Sanchez, B. Lebeau, J. Patarin, *Chem. Rev.* 102 (2002) 4093–4138.
- [14] Y. Wan, D. Zhao, *Chem. Rev.* 107 (2007) 2821–2860.
- [15] Y. Tao, H. Kanoh, L. Abrams, K. Kaneko, *Chem. Rev.* 106 (2006) 896–910.
- [16] A. Matsumoto, H. Chen, K. Tsutsumi, M. Grun, K. Unger, *Micropor. Mesopor. Mater.* 32 (1999) 55–62.
- [17] H.P. Lin, S.F. Cheng, C.Y. Mou, *Micropor. Mesopor. Mater.* 10 (1997) 111–121.
- [18] R. Ryoo, S. Jun, *J. Phys. Chem. B* 101 (3) (1997) 317–320.
- [19] B. Lindlar, A. Kogelbauer, R. Prins, *Micropor. Mesopor. Mater.* 38 (2000) 167–176.
- [20] M. Luechinger, L. Frunz, G.D. Pirngruber, R. Prins, *Micropor. Mesopor. Mater.* 64 (2003) 203–211.
- [21] S. Jun, J.M. Kim, R. Ryoo, Y.-S. Ahn, M.K. Han, *Micropor. Mesopor. Mater.* 41 (2000) 119–127.
- [22] W.J. Kim, J.C. Yoo, D.T. Hayhurst, *Micropor. Mesopor. Mater.* 39 (2000) 177–187.
- [23] Q.-H. Xia, K. Hidajat, S. Kawi, *Mater. Lett.* 42 (2002) 102–107.
- [24] W. Sangchoom, R. Mokaya, *J. Mater. Chem.* 22 (2012) 18872–18878.
- [25] W. Sangchoom, R. Mokaya, *J. Mater. Chem.* 22 (2012) 18872–18878.
- [26] Y. Zhang, D. Wu, Y. Sun, S. Peng, *Mater. Lett.* 55 (1–2) (2002) 17–19.
- [27] Q. Li, Zh. Wu, D. Feng, B. Tu, D. Zhao, *J. Phys. Chem. C* 114 (2010) 5012–5019.
- [28] Y. Han, D.F. Li, L. Zhao, J.W. Song, X.Y. Yang, N. Li, Y. Di, C.J. Li, S. Wu, X.Z. Xu, X.J. Meng, K.F. Lin, F.S. Xiao, *Angew. Chem. Int. Ed.* 42 (2003) 3633–3637.
- [29] Q. Li, Zh. Wu, B. Tu, S.S. Park, Ch.-S. Ha, D. Zhao, *Micropor. Mesopor. Mater.* 135 (2010) 95–104.
- [30] J.C. Wang, Q.F. Liu, Q. Liu, *Micropor. Mesopor. Mater.* 102 (2007) 51–57.
- [31] R.K. Iler, *The Chemistry of Silica: Solubility, Polymerisation, Colloid and Surface Properties and Biochemistry of Silica*, Wiley, New York, 1979.
- [32] S. Ruthstein, V. Frydman, S. Kababya, M. Landau, D. Goldfarb, *J. Phys. Chem. B* 107 (2003) 1739–1748.
- [33] K. Flodstrom, H. Wennrstorm, V. Alfredsson, *Langmuir* 20 (2004) 680–688.
- [34] C.C. Landry, S.H. Tolbert, K.W. Gallis, A. Monnier, G.D. Stucky, P. Norby, J.C. Hanson, *Chem. Mater.* 13 (2001) 1600–1608.
- [35] P. Agren, M. Linden, J.B. Rosenholm, R. Schwarzenbacher, M. Kriechbaum, H. Amenitsch, P. Lagner, J. Blanchard, F. Schuth, *J. Phys. Chem. B* 103 (1999) 5943–5948.
- [36] K. Flodstrom, C.V. Teixeira, H. Amenitsch, V. Alfredsson, M. Linden, *Langmuir* 20 (12) (2004) 4885–4891.
- [37] S.H. Tolbert, C.C. Landry, G.D. Stucky, B.F. Chmelka, P. Norby, J.C. Hanson, A. Monnier, *Chem. Mater.* 13 (2001) 2247–2256.
- [38] D. Grosso, F. Babonneau, P.-A. Albouy, H. Amenitsch, A.R. Balkenende, A. Brunet-Bruneau, J. Rivory, *Chem. Mater.* 14 (2002) 931–939.
- [39] M. Linden, S.A. Schunk, F. Schuth, *Angew. Chem. Int. Ed.* 37 (1998) 821–823.
- [40] S. O'Brien, R.J. Francis, A. Fogg, D. O'Hare, N. Okazaki, K. Kuroda, *Chem. Mater.* 11 (1999) 1822–1832.
- [41] A. Lind, J. Andersson, S. Karlsson, P. Agren, P. Bussian, H. Amenitsch, M. Linden, *Langmuir* 18 (2002) 1380–1385.
- [42] G. Oster, D.P. Riley, *Acta Cryst.* 5 (1952) 272–276.
- [43] K.J. Edler, P.A. Reynolds, J.W. White, D. Cookson, *J. Chem. Soc. Faraday Trans.* 93 (1997) 199–202.
- [44] G.D. Stucky, A. Monnier, F. Schuth, Q. Huo, D. Margolese, D. Kumar, M. Krishnamurthy, P. Petroff, A. Firouzi, M. Janicke, B.F. Chmelka, *Mol. Cryst. Liq. Cryst.* 240 (1994) 187–200.
- [45] S. Inagaki, Y. Sakamoto, Y. Fukushima, O. Terasaki, *Chem. Mater.* 8 (1996) 2089–2095.
- [46] K.J. Edler, P.A. Reynolds, P.J. Branton, F.R. Trouw, J.W. White, *J. Chem. Soc. Faraday Trans.* 93 (1997) 1667–1674.
- [47] J.L. Blin, M. Imperor-Clerc, *Chem. Soc. Rev.* 42 (2013) 4071–4082.
- [48] S. Schacht, M. Janicke, F. Schuth, *Micropor. Mesopor. Mater.* 22 (1998) 485–495.
- [49] L.A. Solovoyov, S.D. Kirik, A.N. Shmakov, V.N. Romannikov, *Micropor. Mesopor. Mater.* 44–45 (2001) 17–23.
- [50] S.D. Kirik, A.A. Dubkov, S.A. Dubkova, O.M. Sharonova, A.G. Anshits, *Zeolites* 12 (1992) 292–298.
- [51] L.A. Solovoyov, O.V. Belousov, A.N. Shmakov, V.I. Zaikovskii, S.H. Joo, R. Ryoo, E. Haddad, A. Gedeon, S.D. Kirik, *Nanotechnol. Mesostruct. Mater. Stud. Surf. Sci. Catal.* 146 (2003) 299–302.
- [52] V.A. Parfenov, S.D. Kirik, *J. Surf. Invest.* 2 (2006) 6–11.
- [53] L.A. Solovoyov, O.V. Belousov, R.E. Dinnebier, A.N. Shmakov, S.D. Kirik, *J. Phys. Chem. B* 109 (2005) 3233–3237.
- [54] L.A. Solovoyov, *Chem. Soc. Rev.* 42 (2013) 3708–3720.
- [55] L.A. Solovoyov, T.-W. Kim, F. Kleitz, O. Terasaki, R. Ryoo, *Chem. Mater.* 16 (2004) 2274–2281.
- [56] F. Kleitz, T. Czuryzskiewicz, L.A. Solovoyov, M. Linden, *Chem. Mater.* 18 (2006) 5070–5079.
- [57] F. Kleitz, L.A. Solovoyov, G.M. Anilkumar, Sh.H. Choi, R. Ryoo, *Chem. Commun.* (2004) 1536–1537.
- [58] L.A. Solovoyov, V.I. Zaikovskii, A.N. Shmakov, O.V. Belousov, R. Ryoo, *Phys. Chem. B* 106 (2002) 12198–12202.
- [59] V.A. Parfenov, S.D. Kirik, *Chem. Sustainable Dev. (Russ.)* 11 (2003) 735–740.
- [60] X.S. Zhao, G.Q. Lu, X. Hu, *Micropor. Mesopor. Mater.* 41 (2000) 37–47.
- [61] R. Ryoo, S. Jun, *J. Phys. Chem. B* 101 (1997) 317–320.
- [62] L.A. Solovoyov, *J. Appl. Cryst.* 37 (2004) 743–749.
- [63] S. Brunauer, P.H. Emmett, E. Teller, *J. Am. Chem. Soc.* 60 (1938) 309–319.
- [64] S.D. Kirik, V.A. Parfenov, *J. Sib. Fed. Univ. Chem.* 4 (1) (2011) 50–72.
- [65] M. Grun, K.K. Unger, A. Matsumoto, K. Tsutsumi, *Micropor. Mesopor. Mater.* 27 (1999) 207–216.
- [66] S.D. Kirik, O.V. Belousov, V.A. Parfenov, M.A. Vershinina, *Glass Phys. Chem.* 31 (4) (2005) 439–451.
- [67] C.J. Gommers, H. Friedrich, M. Wolters, P.E. de Jongh, K.P. de Jong, *Chem. Mater.* 21 (2009) 1311–1317.
- [68] S.A. Kozlova, S.D. Kirik, *Micropor. Mesopor. Mater.* 133 (2010) 124–133.
- [69] H.P. Lin, C.Y. Mou, *Micropor. Mesopor. Mater.* 55 (2002) 69–80.
- [70] M. Imperor-Clerc, P. Davidson, A. Davidson, *J. Am. Chem. Soc.* 122 (2000) 11925–11933.